

## MAGNETOHYDROSTATIC SUNSPOT MODELS FROM DEEP SUBPHOTOSPHERIC TO CHROMOSPHERIC LAYERS

E. KHOMENKO<sup>1,2</sup> AND M. COLLADOS<sup>1</sup>

*Received 2008 June 11; accepted 2008 August 18*

### ABSTRACT

In order to understand the influence of magnetic fields on the propagation properties of waves, as derived from different local helioseismology techniques, forward modeling of waves is required. Such calculations need a model in magnetohydrostatic equilibrium as an initial atmosphere through which to propagate oscillations. We provide a method to construct such a model in equilibrium for a wide range of parameters, for use in simulations of artificial helioseismologic data. The method combines the advantages of self-similar solutions and current-distributed models. A set of models is developed by numerical integration of magnetohydrostatic equations from the subphotospheric to chromospheric layers.

*Subject headings:* MHD — Sun: magnetic fields — sunspots

*Online material:* FITS files

### 1. INTRODUCTION

In recent years, local helioseismology has provided new insights into the subphotospheric structure of quiet and active regions of the Sun (Duvall et al. 1993; Kosovichev 1999, 2002; Kosovichev et al. 2000; Zhao & Kosovichev 2003; Braun & Lindsey 2000). However, the influence of magnetic fields on data interpretation has not been fully explored. Theoretical efforts have been made by Crouch & Cally (2003), Cally (2005, 2006), Schunker & Cally (2006), Cally & Goossens (2007), and Schunker et al. (2008) to include mode conversion and to model the ray paths of waves in magnetized structures by means of analytical theory. These studies confirm the potential importance for helioseismic measurements of the so-called surface effects caused by the presence of a magnetic field. A more complete understanding of the problem perhaps could be reached via direct forward modeling of helioseismological data, since magnetic fields of arbitrary configuration can be used. Several recent works report efforts in this direction, e.g., Gizon et al. (2006), Khomenko & Collados (2006), Parchevsky & Kosovichev (2007), Shelyag et al. (2007), Hanasoge (2008), and Cameron et al. (2008). In all these works (except Shelyag et al. 2007), the authors apply a similar strategy. In particular, they assume the existence of an equilibrium atmosphere containing a magnetostatic structure whose properties may resemble to a larger or lesser extent those of a sunspot or a magnetic flux tube. A small-amplitude perturbation is then applied to the system in order to study wave propagation, wave mode transformations, amplitude and phase behavior of waves in a complex magnetic field topology, etc.

The behavior of waves observed in active regions is very sensitive to their magnetic field configuration. The photosphere and low chromosphere are regions where a small change of parameters, such as the size of the magnetic structure, or its temperature, density, or magnetic field strength and inclination, may produce significant changes in the resulting wave field. Simulations can be of invaluable help in exploring different magnetostatic structures within a full parameter space, in order to understand the ef-

fects produced by the magnetic field on the measurable variables used in local helioseismology.

This task requires a robust procedure to construct magnetostatic structures of desired properties. In this paper, we propose such a strategy, and apply it to obtain thick structures as prototypes for solar spots and pores. As a minimum requirement, the model should fulfill the following conditions: (1) in the photosphere the model should, on average, reproduce the properties of a typical sunspot; (2) at the border, the model should smoothly merge into a quiet-Sun nonmagnetic model atmosphere; (3) it should be possible to choose the profile of thermodynamic parameters at the sunspot axis; (4) Wilson depression should be taken into account; (5) magnetic field strength, inclination, and the radius of the structure should be adjustable; and (6) the model should be easily extensible into an arbitrary depth below the photosphere.

There is a vast literature of work on magnetostatic models. Leaving aside small-scale flux tube models, those for thick structures can be divided into those possessing a current sheet (e.g., Pizzo 1990), with a sharp magnetic-nonmagnetic interface, and those with distributed currents (e.g., Pizzo 1986), showing a smooth transition. Without discussing the advantages and disadvantages of the both, we will proceed here with current-distributed models.

Available current-distributed models generally apply one of two different philosophies. In the first, the magnetic structure is prescribed and the distribution of thermodynamic variables is looked for to be in agreement with this structure. This is the class of self-similar models, as proposed by Schlüter & Temesváry (1958) and then extended by, e.g., Low (1975, 1980). In the second set of models, the pressure distribution is prescribed as the boundary condition at the axis of the magnetic structure and in the distant nonmagnetic atmosphere. Both pressure and magnetic field are iteratively changed in the remaining points to reach an equilibrium situation (Pizzo 1986).

From the point of view of the requirements given above, both classes of models have advantages and disadvantages. The approach of Pizzo (1986) is more fruitful in the photosphere, since the pressure distributions of the field-free and magnetized atmospheres can be taken from observations and are relatively well known. However, for deep subphotospheric layers, models that can be taken as boundary conditions are scarce. More precisely, the quiet-Sun nonmagnetic pressure stratification can be taken

<sup>1</sup> Instituto de Astrofísica de Canarias, 38205 La Laguna, Tenerife, Spain; khomenko@iac.es, mcv@iac.es.

<sup>2</sup> Main Astronomical Observatory, NAS, 03680 Kyiv, Ukraine.

from helioseismological data, for example, from the standard solar model of Christensen-Dalsgaard et al. (1996). As for the sunspot axis, no precise data are available (see, however, Zhao et al. 2001; Kosovichev 2002; Couvidat et al. 2006). The model of Pizzo (1986) turns out to be very sensitive to the pressure deficit inside sunspots, and the method in general has poor convergence if the simulation box is too deep, and is very sensitive to the estimate of the pressure distribution at the sunspot axis. This makes the method unsuitable for our purposes.

On the other hand, the procedure proposed by Low (1980) works better in deep layers, where the gas pressure dominates over the magnetic pressure. In the photosphere, where the plasma becomes magnetically dominated, negative pressures are frequently obtained from the method of Low (1980). It is complicated to guess the parameters of the magnetic field configuration in order to avoid this problem. At the same time, if one wishes to extend the models into the photosphere and higher layers, the magnetic field strength is limited to rather low flux-tube-like values, not appropriate for sunspots (see Hanasoge 2008; Cameron et al. 2008).

In this paper, we take advantage of both Pizzo-like and Low-like approaches, and propose a method to calculate the magnetostatic equilibrium of a thick sunspot-like structure with the properties defined above. Below we describe the equations that allow us to successfully merge results from both methods, and show examples of magnetohydrostatic (MHS) solutions for a wide range of parameters. Conclusions are given in the last section.

## 2. METHOD

We solve the equilibrium force balance equation together with divergence-free condition for the magnetic field:

$$-\nabla P + \rho \mathbf{g} + \frac{1}{4\pi} (\nabla \times \mathbf{B}) \times \mathbf{B} = 0, \quad (1)$$

$$\nabla \cdot \mathbf{B} = 0.$$

Following Pizzo (1986), the equations are solved in cylindrical coordinates  $(r, \phi, z)$ , and axial symmetry is assumed (i.e., all variables are independent of  $\phi$ ). Under these conditions the magnetic field vector can be conveniently written in terms of the field line constant  $u$ ,

$$\mathbf{B} = \left( -\frac{1}{r} \frac{\partial u}{\partial z}, \frac{G(u)}{r}, \frac{1}{r} \frac{\partial u}{\partial r} \right), \quad (2)$$

where  $G(u)$  is a function related to the twist component of the field. The variable  $u$  is used both in Pizzo (1986) and Low (1980). The difference is that in Low (1980) the analytical expression for  $u$  is postulated, while in Pizzo (1986) the shape of the field lines  $u$  is obtained by iteratively solving the equation of the force balance for given boundary conditions in agreement with some pressure distribution. Except for constants, the functional form of  $u$  used by Pizzo (1986) as an initial condition at the lower boundary of the computational domain is exactly the same as that postulated by Low (1980). Thus, both models can be joined in a natural way, assuming that the deep layers of the model sunspot can be approximated by the self-similar solution and the upper layers by the solution of Pizzo.

In Low (1980), following the spirit of self-similar solutions, the field-line constant  $u$  is expressed as a function of one variable,  $\varphi$ :

$$u(r, z) = u(\varphi), \quad \varphi = r^2 F(z), \quad (3)$$

$$F(z) = (z^2 + a^2)^{-1},$$

where  $a$  is a constant parameter. The field is untwisted, and the azimuthal component,  $B_\phi$ , is zero. This is equivalent to setting

$G(u) = 0$  in equation (2). Using the above expression, equation (2) can be rewritten as a function of  $\varphi$ :

$$\mathbf{B} = \left( -r \frac{dF(z)}{dz} \frac{du}{d\varphi}, 0, 2F(z) \frac{du}{d\varphi} \right). \quad (4)$$

Following Low, the function  $du/d\varphi$  has to satisfy certain normalizations in order to fulfill the force balance equation. This leads to the expression

$$\frac{du}{d\varphi} = B_0^L h^2 \exp(-\eta\varphi), \quad (5)$$

where  $B_0^L$  is a parameter that controls the magnetic field strength, and  $h$  is a suitable length scale (although note that Low uses dimensionless variables, while here we choose to use physical dimensions for all the variables).

Introducing equation (5) into equation (4), the horizontal and vertical components of the magnetic field vector in the Low's model can be written as

$$B_r(r, z) = 2B_0^L \frac{(z - z_d) r h^2}{[(z - z_d)^2 + a^2]^2} \exp\left[\frac{-\eta r^2}{(z - z_d)^2 + a^2}\right], \quad (6)$$

$$B_z(r, z) = 2B_0^L \frac{h^2}{(z - z_d)^2 + a^2} \exp\left[\frac{-\eta r^2}{(z - z_d)^2 + a^2}\right]. \quad (7)$$

The parameter  $z_d$  is a reference height, where the magnetic field is purely vertical. Equation (7) is directly comparable to the one used in Pizzo as a boundary condition at the bottom boundary of the domain:

$$B_z(r, z_0) = B_0^P \exp(-r^2/r_e^2). \quad (8)$$

Comparing these two expressions, we see that if the two models are to be joined at some arbitrary height  $z = z_0$ , the parameters of the models should be related as

$$B_0^P = B_0^L \frac{2h^2}{(z_0 - z_d)^2 + a^2}, \quad (9)$$

$$r_e^2 = [(z_0 - z_d)^2 + a^2]/\eta. \quad (10)$$

Keeping this in mind, the model can be constructed following the steps described below.

### 2.1. Step 1: Generation of a Self-Similar Solution in Deep Layers

In deep subphotospheric layers, we calculate a self-similar solution for  $\mathbf{B}$  after equations (6) and (7). The pressure and density distributions with height and radius are found from analytical expressions (eqs. [50] and [51] in Low 1980). As a boundary condition at the right boundary (field-free atmosphere), we take the pressure and density from model S of Christensen-Dalsgaard et al. (1996). The choice of field-free pressure and density is rather arbitrary, however. Because of azimuthal symmetry, the left boundary of the domain corresponds to  $r = 0$ , i.e., the axis of the magnetic structure. The lower boundary is taken exactly at height  $z_d$ , where  $B_r(r, z_d) = 0$  at all distances  $r$ . In all the cases presented here,  $z_d = -10$  Mm, and the origin for the  $z$ -axis is taken at the base of the photosphere. Given pressure and density, the temperature distribution in the model sunspot can be calculated using the equation of state either in tabular form or for an ideal gas. The parameters  $\eta$ ,  $a$ , and  $B_0^L$  can be chosen freely. An additional free

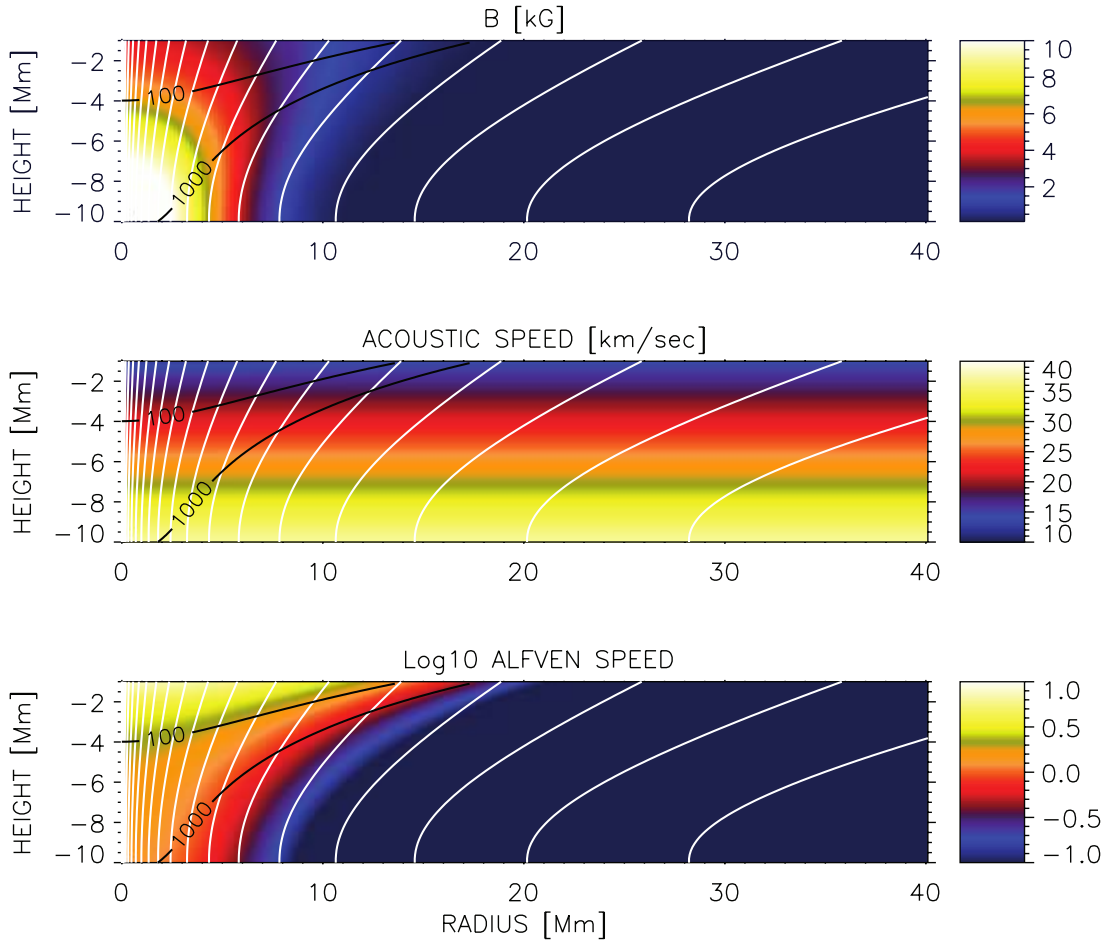


FIG. 1.—Topology of the Low solution with  $a = 2h$ ,  $h = 3$  Mm,  $\eta = 1.3$ ,  $B_0 = 25,000$  G, and  $z_0 = -1$  Mm. *Top*: Magnetic field strength; *middle*: acoustic speed; *bottom*: log of the Alfvén speed. White lines are magnetic field lines. Black lines with labels are the contours of the ratio of the sound speed and the Alfvén speed squared,  $c_s^2/v_A^2$ .

parameter is the height,  $z_0$ , that limits the upper boundary of the self-similar model. Depending on the height of the upper boundary,  $B_0^L$  can be made larger or smaller to prevent giving negative gas pressures.

The basic topology of the solution is given in Figure 1 for the parameters indicated in the figure caption. These parameters are chosen on purpose to demonstrate that the method is able to deal with large field strengths. The sunspot radius at the bottom boundary is roughly defined by  $a\eta^{-1/2}$  (Low 1980). The inclination of the field at the top boundary changes with the distance from the axis, from 0 to about  $70^\circ$  at the rightmost point of the domain. The magnetic field is concentrated inside the first 15 Mm from the axis, being weak in the rest of the domain. The field strength drops at the axis from 12 kG at  $z = -10$  Mm to 4 kG at  $z = -1$  Mm depth. The gas pressure is always above the magnetic pressure.

The Wilson depression is rather weak, and the model sunspot is almost thermally plane-parallel in deep layers, as follows from the distribution of the acoustic speed,  $c_s$ . We do not have criteria to judge how realistic this description is. Data on the subphotospheric distribution of the sound speed in sunspots are scarce and uncertain (see, however, time-distance analysis results by Zhao et al. 2001; Kosovichev 2002; Couvidat et al. 2006).

### 2.2. Step 2: Generation of a Potential Solution in the Overlying Atmosphere

Given the values of  $\eta$ ,  $a$ ,  $B_0^L$ ,  $z_d$ , and  $z_0$ , we calculate the initial parameters of the Pizzo model from equations (9) and (10). This

gives us  $B_0^P = 4$  kG and  $r_e = 9.4$  Mm. We follow the same steps as in the original paper of Pizzo (1986), and start by computing the potential solution,

$$\frac{\partial^2 u}{\partial r^2} - \frac{1}{r} \frac{\partial u}{\partial r} + \frac{\partial^2 u}{\partial z^2} = 0. \quad (11)$$

The bottom boundary of the domain coincides with the top boundary from the previous step and is located at  $z = -1$  Mm, below the photosphere. The field-line constant  $u$  at the bottom boundary can be approximated by

$$u = r_e^2 B_0^P [1 - \exp(-r^2/r_e^2)]/2. \quad (12)$$

At the left (sunspot axis) and top boundaries  $u = 0$  (vertical field), and  $u$  approaches a constant value at the right boundary (horizontal field). With this set of boundary conditions, the boundary value problem posed by equation (11) can be solved by standard methods.

### 2.3. Step 3: Generation of a Magnetostatic Solution in the Overlying Atmosphere

The potential solution obtained in step 2 is used as initial guess in the integration of the complete force balance equation along the magnetic field lines (eq. [4] in the paper by Pizzo):

$$\frac{\partial^2 u}{\partial r^2} - \frac{1}{r} \frac{\partial u}{\partial r} + \frac{\partial^2 u}{\partial z^2} = -4\pi r^2 \frac{\partial P(u, z)}{\partial u}. \quad (13)$$

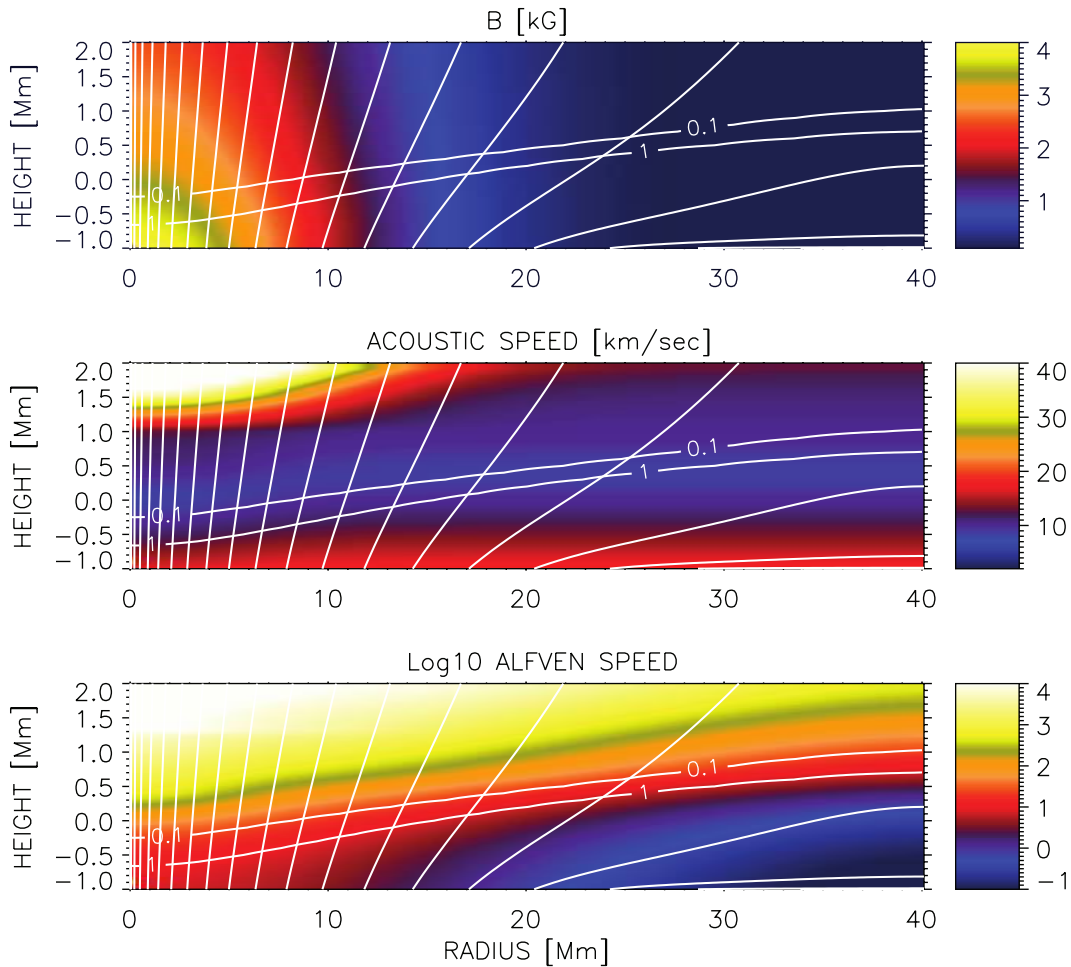


FIG. 2.— Topology of the Pizzo solution with  $B_0^p = 4$  kG and  $r_e = 9.4$  Mm. *Top*: Magnetic field strength; *middle*: acoustic speed; *bottom*: log of the Alfvén speed. White lines are magnetic field lines. White lines with labels are the contours of  $c_s^2/u_A^2$ . Note that for better visualization, the vertical axis has been expanded.

In order to start iterations we need an approximation for the distribution of pressure along the magnetic field lines,  $P(u, z)$ . Following Pizzo (1986) and Low (1975), we take this to be of the form

$$P(u, z) = P_0(u) \exp \left[ - \int_0^z \frac{dz'}{h(u, z')} \right], \quad (14)$$

where  $P_0(u)$  is the gas pressure along the bottom boundary. The function  $h(u, z)$  is a scale height. For a complete description of the problem, the representative pressure distributions along the

axis and in the field-free quiet atmosphere need to be specified. As field-free atmosphere, we use model S of Christensen-Dalsgaard et al. (1996) smoothly joined to the VAL-C model of the solar chromosphere (Vernazza et al. 1981). At the axis, we use the Avrett (1981) model in the upper layers. In deep layers, we adopt a model by Kosovichev et al. (2000) obtained from helioseismic inversions of the sound speed beneath sunspots. This model already takes into account the Wilson depression, which is about 450 km. However, the complete model can be shifted up or down on the axis, if smaller or larger values of the Wilson depression are required. The model

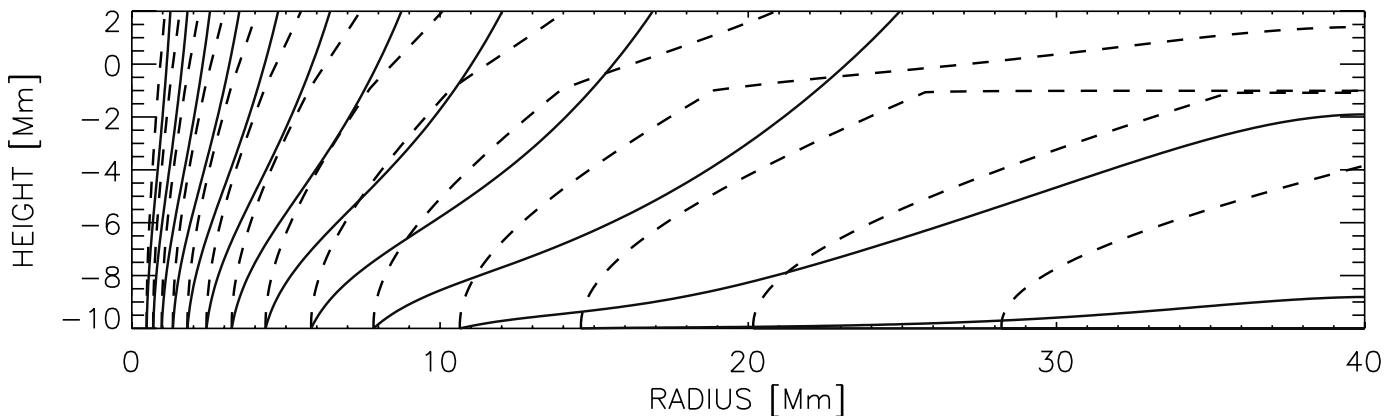


FIG. 3.— Topology of the magnetic field lines before iterations (*dashed lines*) and after a new equilibrium is reached (*solid lines*).

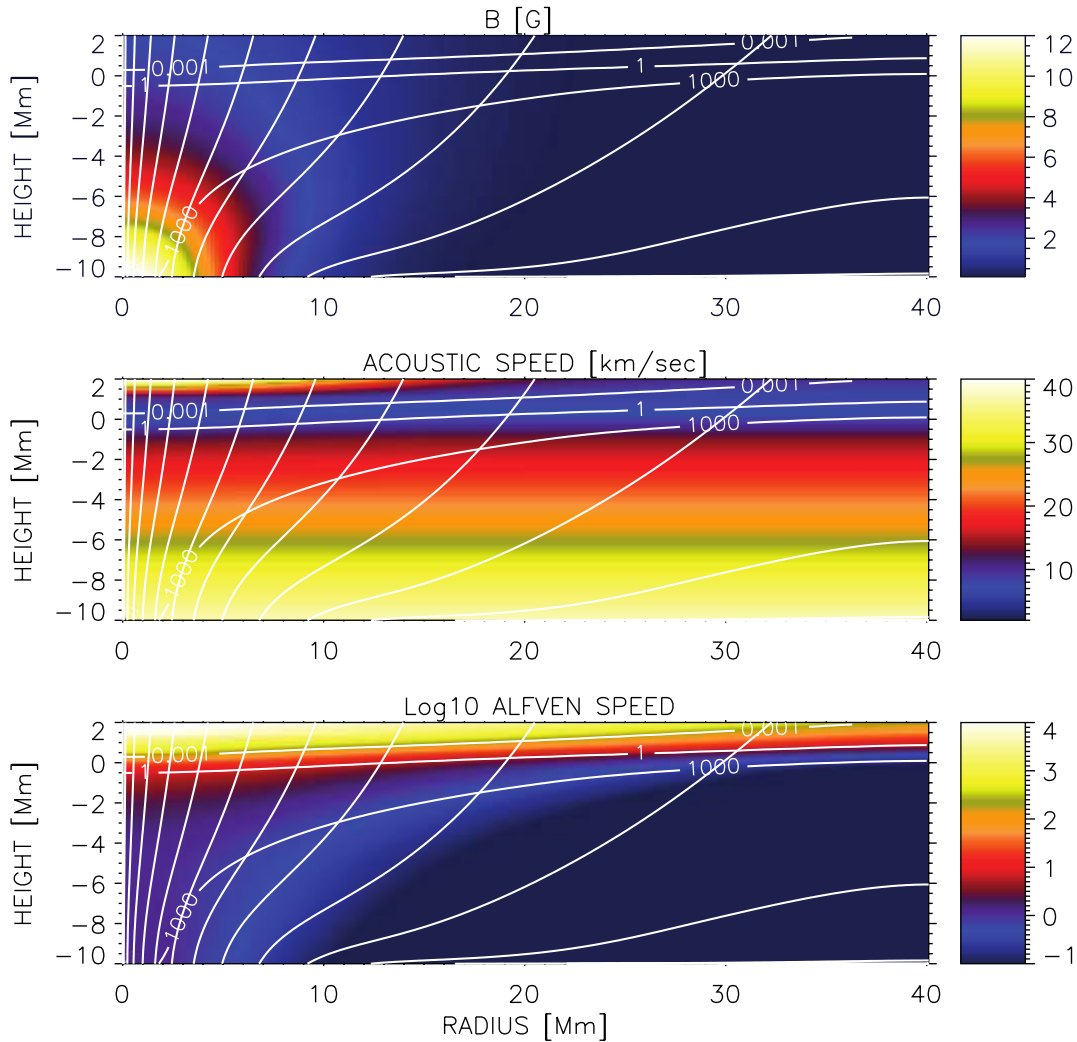


FIG. 4.—Topology of the complete solution with  $B_0^L = 25,000$ ,  $a = 2h$ ,  $h = 3$  Mm, and  $\eta = 1.3$  ( $B_0^P = 4$  kG and  $r_e = 9.4$  Mm). *Top*: Magnetic field strength; *middle*: acoustic speed; *bottom*: log of the Alfvén speed. White lines are magnetic field lines. White lines with labels are the contours of  $c_s^2/v_A^2$ .

has a cool region just below the surface and a hot one below, down to about  $-10$  Mm. For our purposes we take this model starting from  $-1$  Mm depth, and thus the hot layer is not taken into account. Once these models are specified, we calculate a smooth transition between them for the gas pressure  $P(u, z)$  and scale height  $h(u, z)$  distributions, as given by Pizzo (1986) in his equations (13), (17), and (18). Then, equation (13) is iterated until a convergence criterion is reached.

The model sunspot for the parameters given above is shown in Figure 2. The magnetic field on the axis drops from 4 kG at  $z = -1$  Mm to about 2 kG at 2 Mm, which is a rather large value at this height. Due to such a large field strength, the Alfvén speed exceeds  $10^4$  km s $^{-1}$  in the upper layers. The image of the sound shows the presence of the Wilson depression around  $z = 0$ , i.e., the temperature at the sunspot axis is smaller than in the outside atmosphere at a given height. Note that at higher layers, the effect is the opposite, and the temperature inside the sunspot is larger. This effect is due to the initial distribution in the model atmospheres taken as boundary conditions. The field lines are more inclined compared to the Low solution in Figure 1.

#### 2.4. Step 4: Concatenating the Solutions

Both solutions obtained in step 1 and step 3 are in MHS equilibrium. In order to construct the complete model from deep to

high layers, one has to put one model on top of the other. However, despite the fact that  $B_z$  at the bottom boundary of the Pizzo model is calculated to be in agreement with  $B_z$  at the top boundary of the Low model, there is a discontinuity in the horizontal component of the magnetic field. This discontinuity can be appreciated in Figure 3, where the dashed field lines show the two models concatenated as they are. The reason for this discontinuity is twofold. On the one hand, the physics of the solution changes abruptly from one model to the other, thus changing the gradients of the magnetic field, gas pressure, etc. On the other hand, the boundary condition for the field line constant  $u$  is not the same in the both models. In the Low model, there is neither the need nor the possibility to set conditions on  $u$ . The inclination of the magnetic field lines at the right boundary is a consequence of the parameters of the model, and they should not necessarily be horizontal. Contrarily, in the case of the Pizzo model, we impose a horizontal magnetic field at the right boundary. The dependence of  $B_z$  on  $r$  given by equation (8) defines the vertical magnetic field strength but does not put constraints on the horizontal field component.

Thus, in order to obtain a smooth solution everywhere in the domain, we repeat the step 3 calculations for the complete model sunspot. We take the pressure distributions at the axis and in the field-free outside atmosphere from the joint model at all heights.

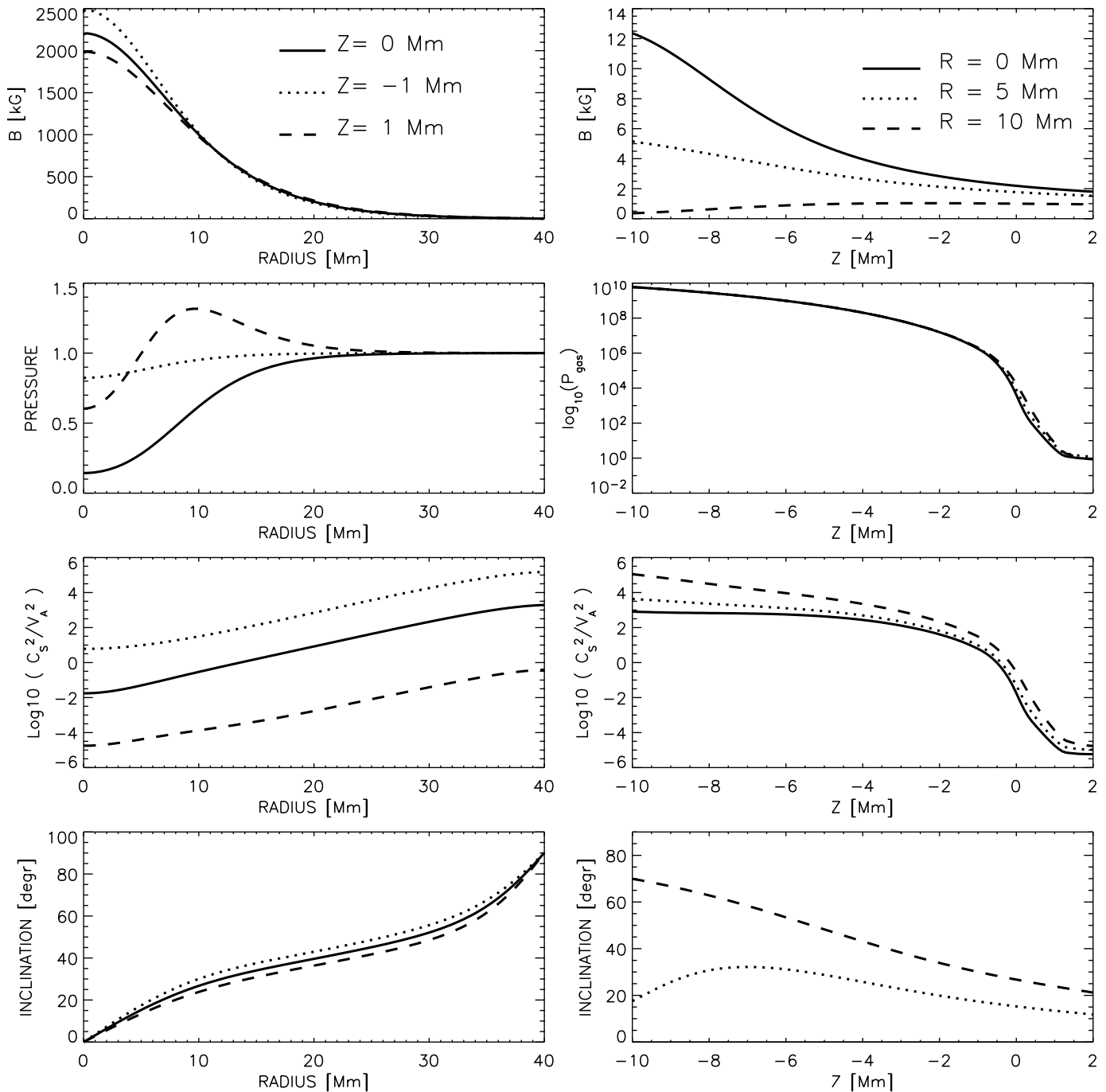


FIG. 5.—Distribution with radial distance (*left panels*) and with depth (*right panels*) of the magnetic field strength, pressure, ratio  $c_s^2/v_A^2$ , and the magnetic field inclination for the sunspot with  $B_0^l = 25,000$ ,  $a = 2h$ ,  $h = 3$  Mm, and  $\eta = 1.3$  (corresponding to  $B_0^p = 4$  kG and  $r_e = 9.4$  Mm at  $z = -1$  Mm). The radial pressure distributions are normalized to their values at the right boundary.

The boundary conditions for  $u$  are the same as in the Pizzo model. The distribution of  $u$  at the bottom boundary is taken from the Low model. Then we repeat the solution of equation (13). The resulting topology of the magnetic field lines is plotted in Figure 3 by solid lines. The field lines in the final solution are more horizontal in low layers, while they are more vertical in the upper layers.

Figure 4 gives the distribution of some parameters in the complete model sunspot, at all layers. We can see that the last iteration has redistributed all the parameters from the individual Low and Pizzo parts of the solution. In particular, the magnetic field gradient at the axis is now steeper, and the field strength in high

layers becomes lower. The field is in general more inclined, being horizontal at the right-hand domain boundary, consistent with our imposed boundary condition there. The gas pressure is modified accordingly to maintain the new force balance.

Figure 5 gives a more detailed view of the model sunspot solution. It shows the distribution with radius (*left panels*) and with depth (*right panels*) of some parameters of the sunspot atmosphere. The field strength decreases rapidly with height at an average rate of about  $1 \text{ G km}^{-1}$  at the axis. The magnitude of the gradient decreases with height and with distance to the axis. These gradients are in agreement with photospheric spectropolarimetric

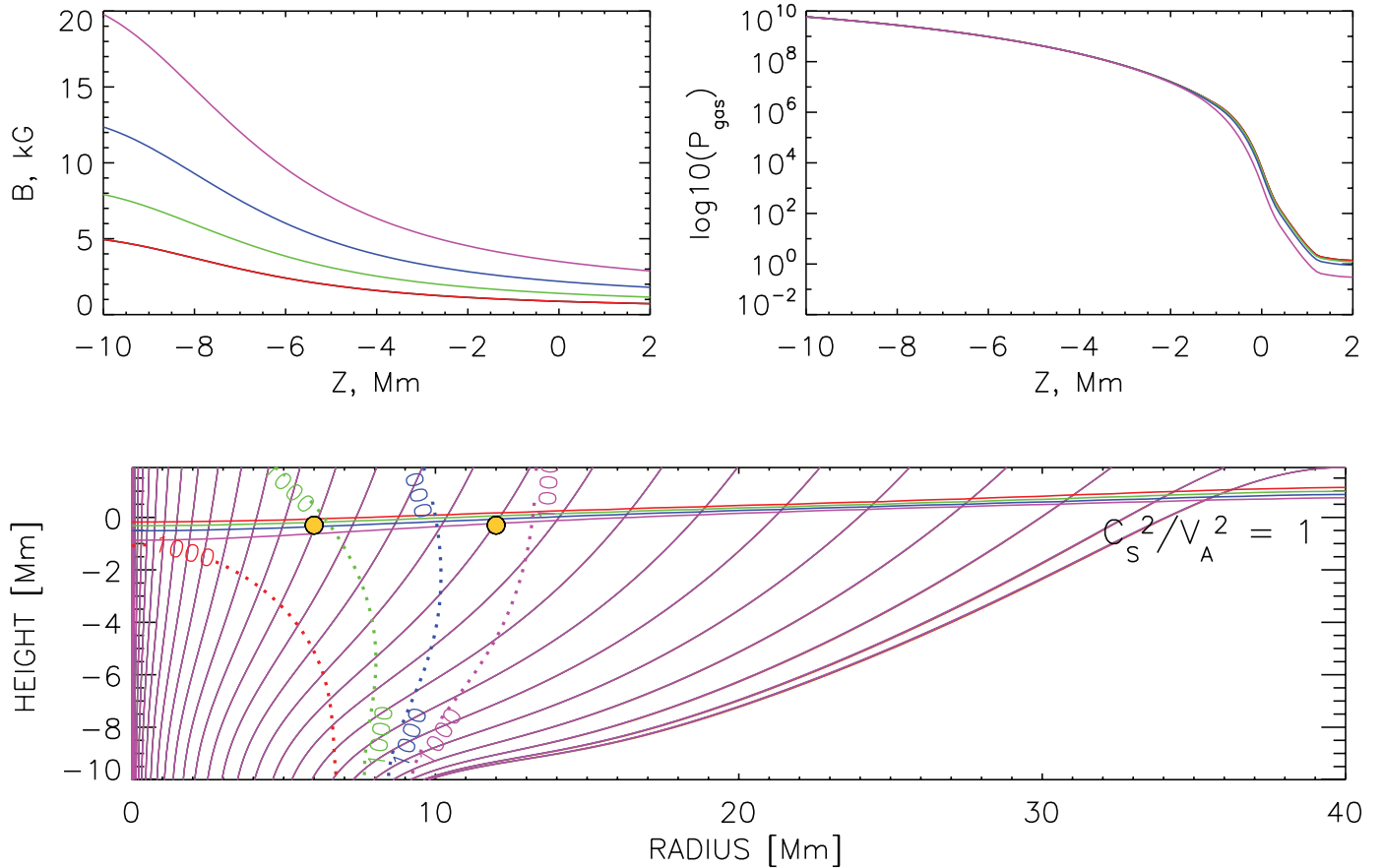


FIG. 6.— *Top panels:* Height dependence of the magnetic field and pressure at the axis for the models with  $a = 2h$ ,  $h = 3$  Mm,  $\eta = 1.3$ , and  $B_0^L = 10,000$  G (red line), 16,000 G (green line), 25,000 G (blue line), and 40,000 G (magenta line). *Bottom panel:* Topology of the magnetic field lines for the same solutions (same color-coding). Contours of the magnetic field strength of  $B = 1000$  G are shown by dotted lines for each case. Horizontal solid lines mark the levels of  $c_s = v_A$ .

observations (Solanki 2003). The magnitude of the pressure deficit inside the model sunspot decreases with depth, almost disappearing at about  $-2$  Mm depth, in accordance with our assumption of self-similarity of the MHS solution at larger depths.

As can be seen from the radial pressure distribution, there is a pressure excess observed at larger heights in the chromosphere at some distance from the axis. This pressure excess would produce a bright ring in the emergent intensity from the model sunspot, and it is present in the original model of Pizzo (1986). As shown in that work, the bright ring can be removed by an improved initial estimate of the  $P(u, z)$  distribution. It is unimportant for the purpose of the present work, since we only need an approximate agreement between the average properties of the MHS solution and the observed properties of sunspots. The magnetic field lines of the model sunspot are inclined less than  $30^\circ$  within the first 10 Mm from the axis, which can be considered as the umbra. Because of the boundary condition, the inclination changes gradually, becoming  $90^\circ$  at the edge of the model, where the magnetic field is already very weak. The ratio between the sound speed and the Alfvén speed squared (which gives the measure of the gas to magnetic pressure) changes by orders of magnitude, from  $10^6$  at  $z = -10$  Mm to  $10^{-6}$  at  $z = 2$  Mm. Note that despite this, there is no problem with the convergence of the solution.

In the next section, we give more examples of MHS solutions, comparing models obtained with various sets of parameters. In the examples below we discuss models calculated in a complete domain from  $z = -10$  to  $z = 2$  Mm.

### 3. EXAMPLES

*Dependence on magnetic field strength.*—Figure 6 shows the magnetic field topology of models with different values of the magnetic field strength (parameter  $B_0^L$ ), all the other parameters being exactly the same. As can be seen by comparing the different curves on the figures, the resulting gas pressure stratifications only differ in the highest layers by the amount of the pressure deficit. The magnetic field topology is indistinguishable in all the cases. This is due to two effects. On the one hand, the self-similar solution in the bottom part of the domain scales with magnetic field strength, i.e., the field line topology does not depend on  $B_0^L$ . On the other hand, the Pizzo solution in the upper part is close to the potential imposed by the solution in the bottom part. The potential solution also scales with the magnetic field strength and is independent of thermodynamic properties. These two effects lead the magnetic topology of the final solution in the complete domain to be independent of  $B_0^L$ . This is a useful property from the point of view of helioseismology simulations. Using a set of models with different magnetic field strength, but otherwise the same, the effects of the magnetic field strength on waves can be checked independently of the effects of the magnetic field inclination.

It should be noted that the above property originates only from the particular choice of the parameters  $a$  and  $\eta$ . This choice produces  $r_e$  large enough that the final solution in the upper part of the domain approaches the potential and becomes almost independent of the pressure distribution  $P(u, z)$  (Pizzo 1986).

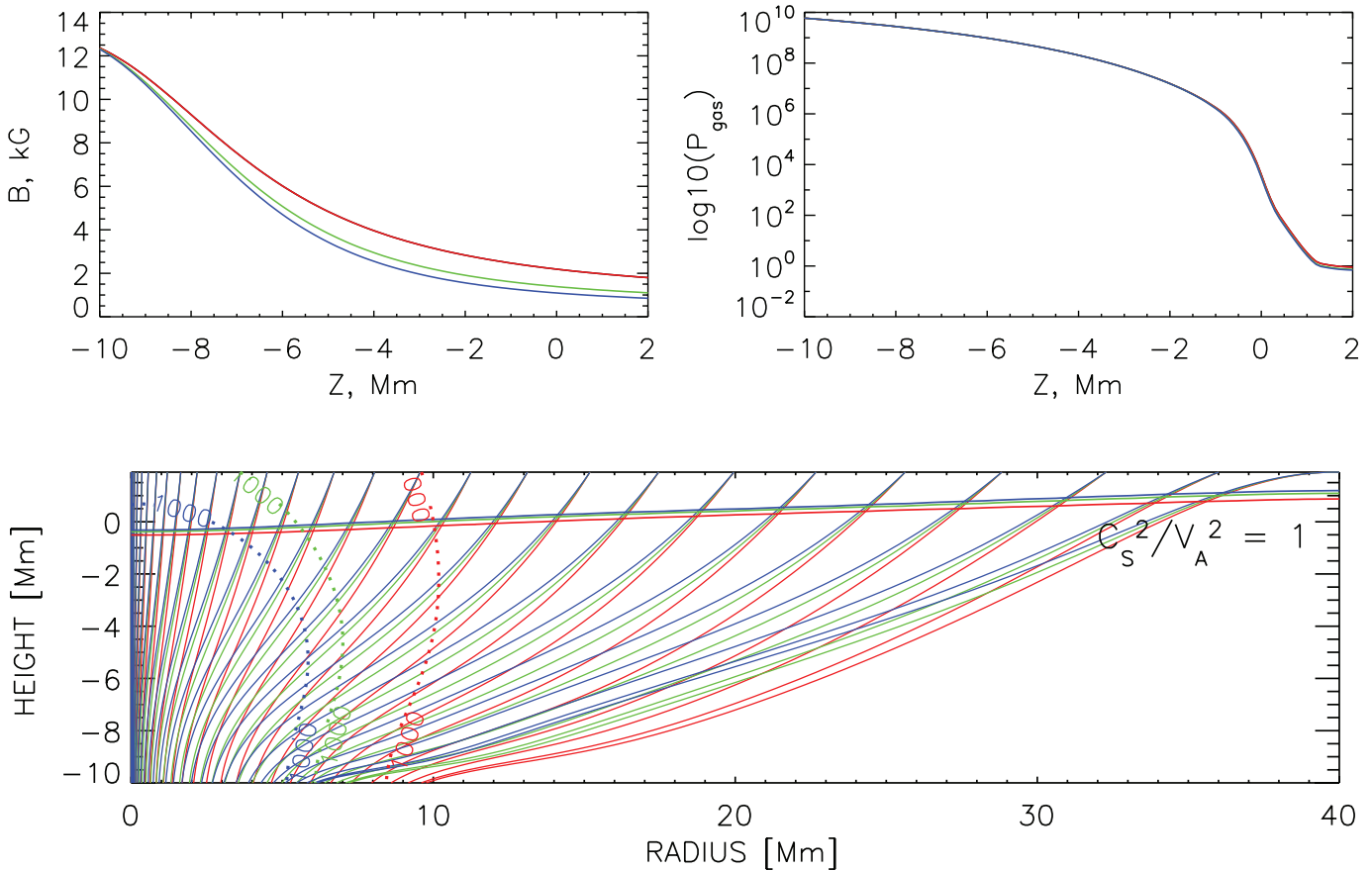


FIG. 7.— *Top panels:* Height dependence of the magnetic field and pressure at the axis for the models with  $a = 2h$ ,  $h = 3$  Mm,  $B_0^L = 25,000$ , and  $\eta = 1.3$  (red line), 2.5 (green line), and 3.5 (blue line). *Bottom panel:* Topology of the magnetic field lines for the same solutions (same color coding). Contours of the magnetic field strength of  $B = 1000$  G are shown by dotted lines for each case. Horizontal solid lines mark the levels of  $c_s = v_A$ .

*Dependence on  $a$  and  $\eta$ .*—Figure 7 shows the magnetic field topology of the models calculated with different values of the parameter  $\eta$  (eqs. [6] and [7]), the rest of the parameters being the same. Note that, according to the above equations, the inclination of the magnetic field is independent of  $\eta$  in the Low model in the bottom part of the domain. However, the initial radius of the structure in the Pizzo part of the solution,  $r_e$  (eq. [10]), depends on  $\eta$ , thus changing the inclination of the magnetic field lines in the upper part of the atmosphere. The final iteration performed in step 4 takes that into account, making the solution in the complete domain dependent on  $\eta$ .

The change of  $\eta$  produces two effects. By increasing  $\eta$ , we decrease the magnetic field strength by a smaller amount than by varying  $B_0^L$ , as in the previous example. At the same time, increasing  $\eta$  produces an increase of the inclination of the magnetic field lines in the solution in the complete domain. The difference in the inclination is more pronounced in the deep layers of the model. The magnetic field topology of the solutions is different. The gradient of the magnetic field at the axis is slightly larger for larger values of  $\eta$  in the subphotospheric part of the model. Again, this difference is produced after the final iteration in step 4, since the  $B_z(r = 0)$  given by equation (7) of the Low part of the solution is independent of  $\eta$ . The pressure distribution at the axis and the amount of the pressure deficit are not very different between the given models.

Varying the parameter  $a$  produces similar effects. The difference is that by varying  $a$ , we change mostly the curvature of the magnetic field lines and the radius of the structure, without much affecting the magnetic field strength.

*Dependence on  $z_0$ .*—Another parameter introduced in our modeling is the height where both solutions merge,  $z_0$ . Figure 8 shows the topology of the magnetic field lines and the pressure and density distributions with height at the axis for three models with different values of  $z_0$ . In this example we take different values of  $a$  and  $\eta$  in order to produce a structure with a smaller radius. In this way, we show that the procedure is robust and can produce magnetic structures with very different properties.

The magnetic field strength at the axis is almost independent of the choice of  $z_0$ . The amount of the pressure deficit at the near-surface layers increases with decreasing  $z_0$  from  $-1$  to  $-3$  Mm, extending to larger depths. Note, however, that we cannot shift the level of  $z_0$  much deeper than  $-3$  Mm, due to a poor convergence of the solution. Despite the fact that the magnetic field strength is nearly the same, the position of the  $\beta = 1$  level is different in all the solutions due to the different amount of the pressure deficit.

The inclination of the magnetic field lines is similar in the central part of the model sunspots in the three solutions. At the periphery, especially at larger depths, the field lines are more inclined with decreasing  $z_0$ . Thus, the field is more concentrated toward the central part, and the effective radius of the structure is smaller. All models presented in this section are available as FITS files accompanying the electronic edition of this article.

#### 4. CONCLUSIONS

In this study, we propose a method to construct a magnetostatic structure with the properties and size of a typical sunspot, from the deep interior to the solar surface. Previously published methods for constructing such a model have failed due to a poor knowledge

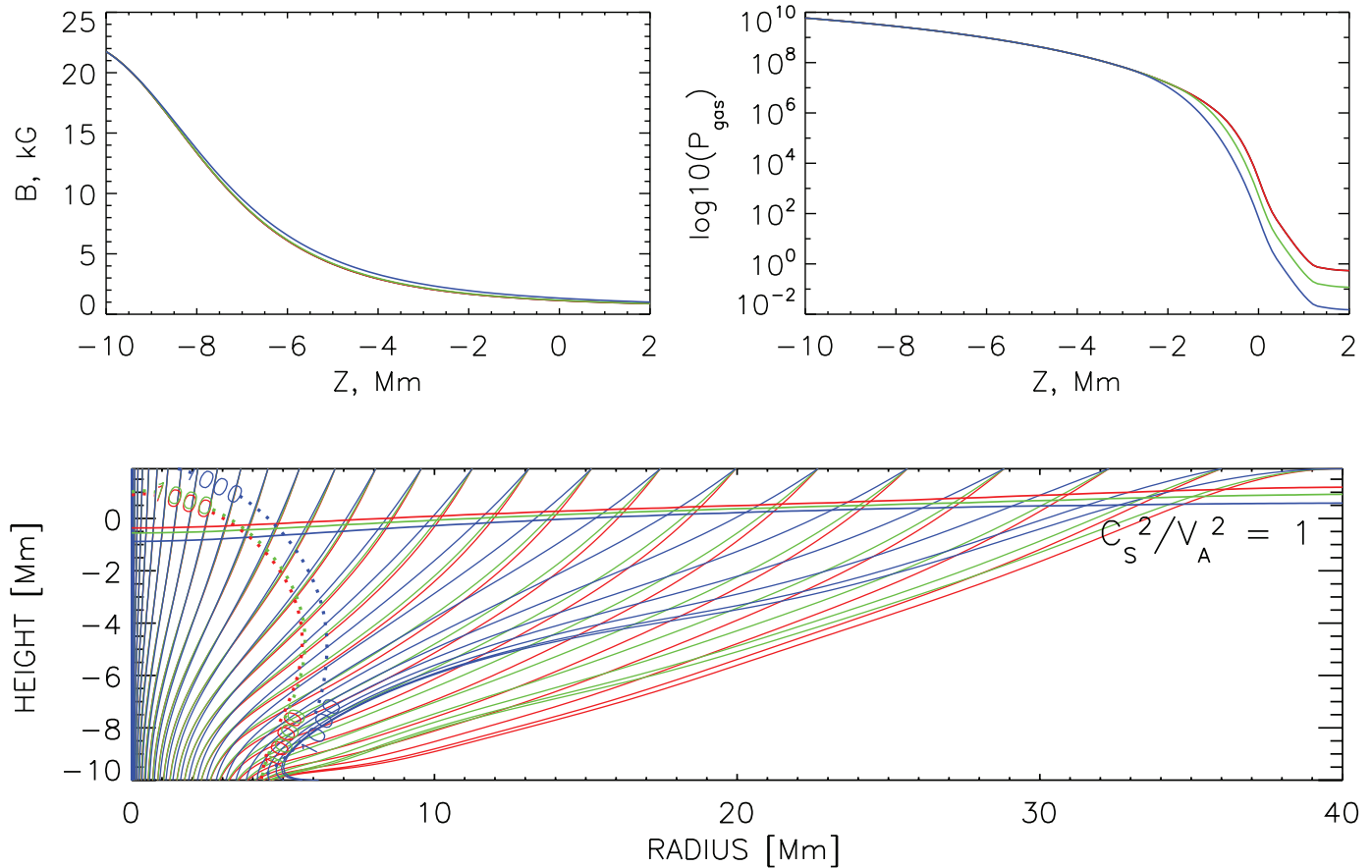


FIG. 8.— *Top panels:* Height dependence of the magnetic field and pressure at the axis for the models with  $a = 1.5h$ ,  $h = 3$  Mm,  $B_0^l = 25,000$ ,  $\eta = 3.5$ , and  $z_0 = -1$  Mm (red line),  $-2$  Mm (green line), and  $-3$  Mm (blue line). *Bottom panel:* Topology of the magnetic field lines for the same models (same color-coding). Contours of the magnetic field strength of  $B = 1000$  G are shown by dotted lines for each case. Horizontal solid lines mark the levels of  $c_s = v_A$ .

of the thermodynamic and magnetic parameters of sunspots in subphotospheric layers. We make use of self-similar models in deep layers and show that such models can naturally merge with models in which the pressure distribution is prescribed on the axis, as well as the field-free atmosphere, allowing for a more realistic description of the atmospheric layers of sunspots. This procedure shows a rather good convergence and stability. By changing the parameters of the solution, a set of models with the desired properties can be produced. We suggest that these models could be used in artificial helioseismology data simulations, among other

applications. Given a set of models, a parametric study can be done investigating the influence of the topology and strength of the magnetic field of sunspots on the parameters inferred by local helioseismology measurements in solar active regions.

This research has been funded by the Spanish Ministerio de Educación y Ciencia through projects AYA2007-63881 and AYA2007-66502.

#### REFERENCES

- Avrett, E. H. 1981, in *The Physics of Sunspots*, Vol. 257 (Sunspot: Sacramento Peak Obs.), 235
- Braun, D. C., & Lindsey, C. 2000, *Sol. Phys.*, 192, 285
- Cally, P. 2005, *MNRAS*, 358, 353
- . 2006, *Philos. Trans. R. Soc. A*, 364, 333
- Cally, P. S., & Goossens, M. 2007, *Sol. Phys.*, in press
- Cameron, R., Gizon, L., & Duvall, T. L. J. 2008, *Sol. Phys.*, in press
- Christensen-Dalsgaard, J., et al. 1996, *Science*, 272, 1286
- Couvidat, S., Birch, A. C., & Kosovichev, A. G. 2006, *ApJ*, 640, 516
- Crouch, A. D., & Cally, P. S. 2003, *Sol. Phys.*, 214, 201
- Duvall, T. L. J., Jefferies, S. M., Harvey, J. W., & Pomerantz, M. A. 1993, *Nature*, 362, 430
- Gizon, L., Hanasoge, S. M., & Birch, A. C. 2006, *ApJ*, 643, 549
- Hanasoge, S. M. 2008, *ApJ*, 680, 1457
- Khomenko, E., & Collados, M. 2006, *ApJ*, 653, 739
- Kosovichev, A. G. 1999, *J. Comput. Appl. Math.*, 109, 1
- . 2002, *Astron. Nachr.*, 323, 186
- Kosovichev, A. G., Duvall, T. L. J., & Scherrer, P. H. 2000, *Sol. Phys.*, 192, 159
- Low, B. C. 1975, *ApJ*, 197, 251
- . 1980, *Sol. Phys.*, 67, 57
- Parchevsky, K. V., & Kosovichev, A. G. 2007, *ApJ*, 666, L53
- Pizzo, V. J. 1986, *ApJ*, 302, 785
- . 1990, *ApJ*, 365, 764
- Schlüter, A., Temesváry, S. 1958, in *IAU Symp. 6, Electromagnetic Phenomena in Cosmical Physics*, Vol. 6, ed. B. Lehnert (Cambridge: Cambridge Univ. Press), 263
- Schunker, H., Braun, D. C., Lindsey, C., & Cally, P. S. 2008, *Sol. Phys.*, in press
- Schunker, H., & Cally, P. S. 2006, *MNRAS*, 372, 551
- Shelyag, S., Erdélyi, R., & Thompson, M. J. 2007, *A&A*, 469, 1101
- Solanki, S. K. 2003, *A&A Rev.*, 11, 153
- Vernazza, J. E., Avrett, E. H., & Loeser, R. 1981, *ApJS*, 45, 635
- Zhao, J., & Kosovichev, A. G. 2003, *ApJ*, 591, 446
- Zhao, J., Kosovichev, A. G., & Duvall, T. L. J. 2001, *ApJ*, 557, 384